

Path integral derivation of the thermofield double state in causal diamonds

Abhijit Chakraborty¹, Carlos R. Ordóñez²
and Gustavo Valdivia-Mera²

¹ Institute for Quantum Computing, University of Waterloo, Waterloo, ON, N2L 3G1, Canada

² Department of Physics, University of Houston, Houston, Texas 77204-5005, USA

E-mail: abhijit.chakraborty@uwaterloo.ca, cordonez@central.uh.edu, gvaldiviamera@uh.edu

May 2024

Abstract. In this article, we follow the framework given in the article *Physica A*, **158**, pg 58-63 (1989) by R. Laflamme to derive the thermofield double state for a causal diamond using the Euclidean path integral formalism, and subsequently derive the causal diamond temperature. The interpretation of the physical and fictitious system in the thermofield double state arises naturally from the boundary conditions of the fields defined on the Euclidean sections of the cylindrical background geometry $S_\beta^1 \times \mathbb{R}$, where β defines the periodicity of the Euclidean time coordinate and S_β^1 is a circumference of length β . The temperature detected by a static diamond observer at $x = 0$ matches with the thermofield double temperature derived via this path integral procedure.

1. Introduction

Stephen Hawking, in his seminal work in 1975, showed that black holes can emit thermal radiation if one considers quantum effects [1]. Hawking's results [1–3] were subsequently corroborated by a series of papers by Unruh, Fulling, Davies, Parker, and Wald [4–10], which flourished into a new field of research on quantum effects in curved spacetime.

Around the same time, Umezawa and Takahashi, motivated by studies in many-body physics, developed the thermofield dynamics formalism, in which they constructed a temperature-dependent vacuum state denoted as $|0(\beta)\rangle$, the thermofield double state (TFD) [11–14]. The purpose of this state was to meet the requirement that the vacuum expectation value for any observable would be numerically equal to the statistical average obtained for an ensemble in thermal equilibrium. In other words, $\langle 0(\beta) | F | 0(\beta) \rangle = Z^{-1}(\beta) \sum_n e^{-\beta E_n} \langle n | F | n \rangle$, where F represents an observable, E_n are energy eigenvalues, and $Z(\beta)$ is the partition function. To accomplish this goal, they introduced a fictitious dynamical system mirroring the original system. Through this approach, they showed that the ‘thermal’ vacuum state fulfilling the desired condition can be expressed as $|0(\beta)\rangle = Z^{-1/2}(\beta) \sum_n e^{-\beta E_n/2} |n, \tilde{n}\rangle$, where $|\tilde{n}\rangle$

is the energy eigenstate of the field defined on the fictitious system.

Shortly after Umezawa and Takahashi's introduction of thermofield dynamics, Israel showed that one can interpret the vacuum state for a scalar field theory defined on extensions of Schwarzschild and Rindler spacetimes – Kruskal and Minkowski, respectively – as the Umezawa-Takahashi's thermofield double state (TFD) [15]. Time-reversed copies of Rindler and Schwarzschild geometries can be identified within these extended spacetimes. It is precisely on these copies that the fictitious fields are defined. Since an observer restricted in the Rindler and Schwarzschild spacetime will only have access to the original system, the degrees of freedom of the fictitious system need to be averaged over, which gives rise to the thermal behavior of the Minkowski or Kruskal vacuum. In other words, the emergence of the thermal behavior in the TFD takes place when the observation of particle modes is restricted due to the presence of horizons. The temperature of the TFD state is usually determined by the intrinsic parameters of the system, such as surface gravity or acceleration in the Schwarzschild and Rindler case, respectively.

In a series of beautiful papers, Laflamme later showed that the TFD can be obtained through the path integral approach [16, 17]. In this context, the field's boundary conditions are set on Euclidean sections obtained by unwrapping the original manifold, where the identification of the Euclidean time $\tau \sim \tau + \beta$ takes place. This identification, typically associated with the periodicity of the polar plane, $\theta \sim \theta + 2\pi$, is necessary to avoid conical singularities and maintain the smoothness of the geometry. Additionally, the periodicity β holds a deeper significance as it bridges the gap between geometry and thermodynamics. When working within Euclidean sections and developing the field theory, we find that this value precisely corresponds to the inverse of the temperature of the ensemble described by the TFD.

Our goal in this article is to apply the elegant methodology developed by Laflamme to the causal diamond (CD) [18, 19]. Unlike the Unruh-Davis effect, in this case, the observers remain stationary at the origin. However, they are subjected to a finite lifetime. This condition gives rise to past and future horizons defining the CD. As Israel noted, the presence of these horizons generates a thermal spectrum. This is due to the limited access to particle modes, causing the physical system to manifest as a mixed quantum state. Causal diamonds provide an interesting insight into the Unruh-like radiation phenomenon because they highlight the sole role of the horizon in thermality in the absence of acceleration. The thermal effect also has a better chance of being detected in tabletop experiments due to the fact that measuring the effect does not require means to create an absurdly high acceleration. Due to these reasons, and its close connection to both black hole physics and quantum many-body theory, causal diamonds have seen a recent upsurge of interest in the community [20–30].

Our article is organized in the following way. In section 2, we provide a brief summary of the framework used by Laflamme to set up our calculations. In section 3, we analyze the Euclidean action of the scalar field defined on the background given by the causal diamond and, through suitable transformations, we adapt it into a recognizable form for subsequent calculations, leading us to the TFD. In section 4, we compute the density matrix of the original physical system and demonstrate that the initially imposed geometric conditions allow us to calculate the equilibrium

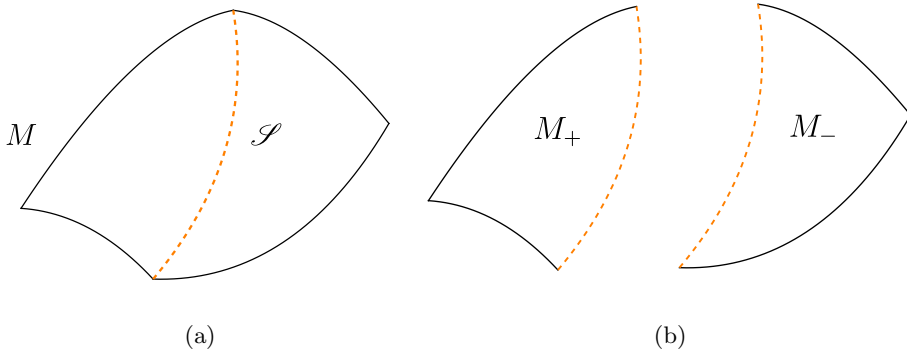


Figure 1: (a) Manifold M and surface \mathcal{S} . (b) Submanifolds M_+ and M_- .

temperature of the thermal bath in a few steps. Finally, we conclude with a discussion on this framework in section 5.

2. Brief review of the geometric interpretation of a TFD state

In this section, we provide a brief overview of the method used by Laflamme in refs. [16, 17] to elucidate the connection between geometry and the thermofield double structure of the vacuum state.

2.1. Euclidean Formalism

In quantum field theory on Euclidean manifolds, the basic assumption is that the probability density for a certain configuration of the fields is proportional to $e^{-S_E[\Phi]}$, where $S_E[\Phi]$ represents the Euclidean action of the field Φ . Thus, the probability that the field possesses a certain property A is given by

$$P(A) = \int_{\mathcal{C}} D\Phi \Pi(A) e^{-S_E[\Phi]}. \quad (1)$$

Here, $\Pi(A)$ equals 1 if the field possesses the mentioned property or zero otherwise, and \mathcal{C} is the class of regular fields defined on the background manifold M , meaning they do not contain singularities at any point in spacetime and their derivatives are smooth everywhere. In the method developed by Laflamme, the property A is defined as the existence of a surface \mathcal{S} that divides M into two parts, M_{\pm} (see figure 1), such that the field has the value $\tilde{\Phi}$ on that surface. Moreover, given that both submanifolds M_{\pm} share this property, $P(A)$ will have contributions from S_E on both submanifolds. In other words, the probability can be factorized into the product of two wave functions,

$$P(A) = \Psi_+(A) \Psi_-(A), \quad (2)$$

where $\Psi_{\pm}(A)$ provides us with the standard calculation of the transition amplitude for the field states defined at the integration limits of the path integral through the Euclidean time evolution operator.

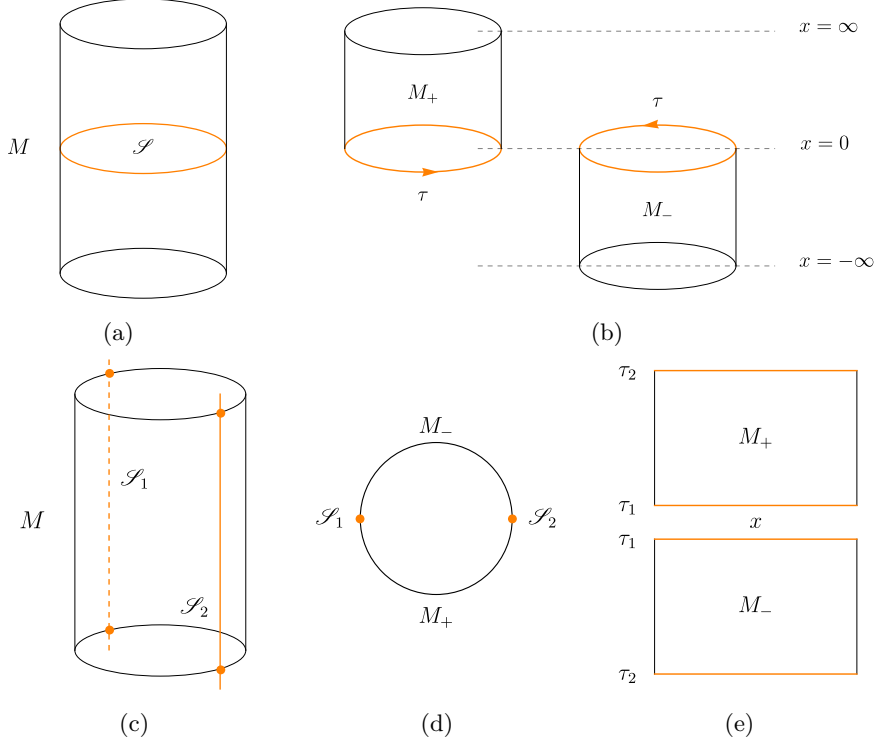


Figure 2: (a) Manifold M given by the cylinder $S_\beta^1 \times \mathbb{R}$ and surface \mathcal{S} . (b) Submanifolds M_+ and M_- obtained through $\mathcal{S} = x$. (c) Manifold M given by the cylinder $S^1 \times \mathbb{R}^1$ and the surfaces \mathcal{S}_1 and \mathcal{S}_2 . (d) Transversal view of the cylinder. (e) Submanifolds M_+ and M_- obtained through $\{\mathcal{S}_1 = \tau_1, \mathcal{S}_2 = \tau_2\}$.

2.2. The cylinder

Let us consider the flat Euclidean manifold M given by $ds^2 = d\tau^2 + dx^2$, represented as the cylinder $S_\beta^1 \times \mathbb{R}$, where τ coordinate is identified to have a periodicity of β . As mentioned earlier, the Laflamme method necessitates the manifold to be divisible into two parts. In this case, we have two straightforward choices:

(1) The foliation $\mathcal{S} = x$, for constant x (figure 2a), provides us with two cylinders similar to the original one. Moreover, by identifying x and τ with the Lorentzian metric $ds^2 = -dx_L^2 + d\tau^2$ via $x = ix_L$, the transition amplitudes for the states defined on the foliations $x = 0$ and $x \rightarrow \infty$, in the left cylinder in figure 2b, and in $x \rightarrow -\infty$ and $x = 0$, in the right one, denoted by Ψ_\pm , will have ground states as their main contribution since in both cases the evolution occurs for $\Delta x \rightarrow \infty$,

$$\langle \phi' | e^{-H\Delta x} | \phi \rangle = \sum_n \langle \phi' | n \rangle \langle n | \phi \rangle e^{-E_n \Delta x} \approx \phi'_0 \phi_0 e^{-E_0 \Delta x}. \quad (3)$$

In the subsequent section, we will demonstrate that the temperature is associated with the inverse of the time interval length; therefore, since the interval Δx is infinite in (3), we have $T = 0$.

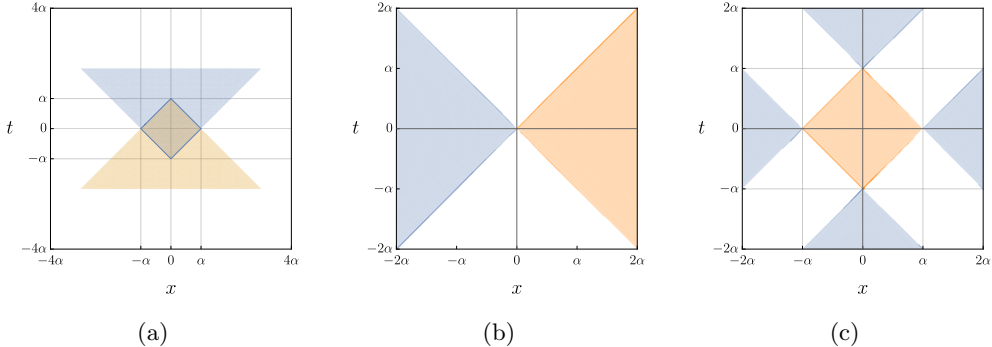


Figure 3: (a) Causal diamond formation for a lifetime of 2α . (b) Left and right Rindler wedges. (c) Interior and exterior regions of the causal diamond.

(2) The foliations $\{\mathcal{S}_1 = \tau_1, \mathcal{S}_2 = \tau_2\}$, where $\tau_2 = \tau_1 + \beta/2$, allow us to unroll the cylinder and divide the manifold M into two equal parts M_+ and M_- (see figures 2c, 2d and 2e). Precisely having the disconnected surfaces $\{\mathcal{S}_1, \mathcal{S}_2\}$ will justify the fictitious field introduced by Umezawa and Takahashi. Furthermore, associating this choice with the Lorentzian metric $ds^2 = -dt^2 + dx^2$ via $\tau = it$, enables us to identify the path integral with the ground state of the field given by a thermal bath at temperature $T = \beta^{-1}$. This will be employed to calculate the temperature of the causal diamond in section 4.

It is precisely the second option that will be the focus of our interest. Thus, the boundary condition of the field on $\{\mathcal{S}_1, \mathcal{S}_2\}$ will be given by $\tilde{\Phi} = \Phi_1$ on \mathcal{S}_1 and $\tilde{\Phi} = \Phi_2$ on \mathcal{S}_2 . Similarly, the Euclidean path integrals on each submanifold are

$$\Psi_+[\Phi_1, \Phi_2] = \int_{\mathcal{C}_+} D\Phi e^{-S_E[\Phi]}, \quad \Psi_-[\Phi_1, \Phi_2] = \int_{\mathcal{C}_-} D\Phi e^{-S_E[\Phi]}. \quad (4)$$

The probability of having the configuration $\tilde{\Phi} = \{\Phi_1, \Phi_2\}$ over $\mathcal{S} = \{\mathcal{S}_1, \mathcal{S}_2\}$ is

$$P_{\mathcal{S}}[\tilde{\Phi}] = \Psi_+[\Phi_1, \Phi_2] \Psi_-[\Phi_1, \Phi_2]. \quad (5)$$

3. Thermofield Double State in Causal Diamonds

The causal diamond is the spacetime region defined by the intersection of the past light cone corresponding to the death event, and the future light cone corresponding to the birth event of an observer with a finite lifetime given by 2α (figure 3a). In this section, we are employing the coordinate transformation defined in [31], which is derived from the more general transformation shown in [32] for a scale factor given by $\lambda = 1$, and by rescaling the Minkowski and Causal Diamond coordinates. Thus, the mapping used is a combination of a special conformal transformation and a spatial translation,

$$(t_d, x_d) = T(-\alpha) \circ K\left(\frac{1}{2\alpha}\right)(t_r, x_r), \quad (6)$$

where

$$K(s) x^\mu = \frac{x^\mu + \delta_1^\mu s x^2}{1 + 2s x^1 + s^2 x^2}, \quad T(a) x^\mu = (x^0, x^1 + a). \quad (7)$$

Here, (t_d, x_d) are the points in Minkowski spacetime restricted to the interior of the causal diamond (figure 3c), and (t_r, x_r) are those restricted to the right Rindler wedge (figure 3b). $K(s)$ represents a special conformal transformation, whose effect is to compactify the unbounded right Rindler wedge into a diamond of size s^{-1} while keeping the causal structure unchanged. The spatial transformation is denoted by $T(a)$, which laterally shifts the diamond to the origin by an amount a . δ_λ^μ is the Kronecker delta function and the superscript 1 denotes the spatial component. Let us use the following coordinate transformation between Minkowski and Rindler, in which $\xi > 0$ and $-\infty < \tau < \infty$,

$$t_r = \xi \sinh(\tau/\alpha), \quad x_r = \xi \cosh(\tau/\alpha). \quad (8)$$

Furthermore, it is important to note that the mapping between the left Rindler wedge (figure 3b) and what we call the external region of the causal diamond (blue-colored region in figure 3c) is achieved by substituting $t_r \rightarrow -t_r$ and $x_r \rightarrow -x_r$, i.e., through parity and time-reversal transformations, in (8).

In Euclidean signature, obtained by $\tau \rightarrow -i\tau$ (and considering from now on τ as Euclidean coordinate), the line element for the causal diamond is conformal to Rindler,

$$ds^2 = \Omega^2(\tau, \xi) \left[\frac{\xi^2}{\alpha^2} d\tau^2 + d\xi^2 \right], \quad (9)$$

where the conformal factor is given by

$$\Omega^2(\tau, \xi) = \frac{16\alpha^4}{(4\alpha\xi \cos(\frac{\tau}{\alpha}) + \xi^2 + 4\alpha^2)^2}. \quad (10)$$

Let us consider the Euclidean action of a real scalar field on a two-dimensional manifold,

$$S_E[\phi] = \frac{1}{2} \int \sqrt{g} d^2x [g^{\mu\nu} \partial_\mu \phi \partial_\nu \phi + m^2 \phi]. \quad (11)$$

Taking the geometry described by $g_{\mu\nu}$ as the line element (9), thus, the Euclidean action (11) takes the following form:

$$S_E[\phi] = -\frac{1}{2} \int d\xi d\tau \phi \left[\frac{\alpha}{\xi} \partial_\tau^2 + \frac{1}{\alpha} \partial_\xi + \frac{\xi}{\alpha} \partial_\xi^2 - m^2 \frac{\Omega^2 \xi}{\alpha} \right] \phi. \quad (12)$$

Let us set $m = 0$ and $\xi = \alpha e^{\rho/\alpha}$ in the Euclidean action (12), such that $0 < \rho < \infty$. Thus, we obtain

$$S_E[\phi] = -\frac{1}{2} \int d\rho d\tau \phi [\partial_\tau^2 + \partial_\rho^2] \phi. \quad (13)$$

A highly noteworthy observation regarding the action (13) is that its form remains unchanged as if its coordinates were from Euclidean space. This stems from the fact that the action in (11) with $m = 0$ is invariant under conformal transformations of the metric, i.e., it is a CFT. We find that transformations

$$g^{\mu\nu} \rightarrow \Omega^{-2} g^{\mu\nu}, \quad \sqrt{g} \rightarrow \Omega^2 \sqrt{g}, \quad \phi \rightarrow \phi, \quad (14)$$

leave the action invariant,

$$S_E[\phi] = \frac{1}{2} \int \sqrt{g} d^2x g^{\mu\nu} \partial_\mu \phi \partial_\nu \phi \rightarrow \frac{1}{2} \int d^2x \Omega^2 \sqrt{g} \Omega^{-2} g^{\mu\nu} \partial_\mu \phi \partial_\nu \phi = S_E[\phi]. \quad (15)$$

Furthermore, from the Fourier transformation of the scalar field,

$$\phi(\tau, \rho) = \frac{1}{\sqrt{2\pi}} \int e^{i\rho\lambda} \phi(\tau, \lambda) d\lambda, \quad (16)$$

in the action (13), we have

$$S_E[\phi] - \frac{1}{2} \int d\tau d\lambda \phi(\tau, \lambda) [\partial_\tau^2 - \lambda^2] \phi^*(\tau, \lambda). \quad (17)$$

It is important to mention that in the Euclidean signature, we have considered periodicity in the time coordinate τ , such that $\tau \in [0, \beta]$. This, as mentioned in section 2.2, is an important requirement of the Laflamme method.

Thus, by discretizing the path integral (see Appendix A), we find that the Euclidean action for each value of λ corresponds to that of the harmonic oscillator,

$$S_E[\psi_\lambda] = -\frac{1}{2} \int_{M_\pm} d\tau \psi_\lambda(\tau) [\partial_\tau^2 - \lambda^2] \psi_\lambda(\tau). \quad (18)$$

Following Laflamme's method and considering the integral (18) defined over M_+ , where the difference in integration limits is given by $\beta/2 = \tau_2 - \tau_1$, and due to the quadratic nature of the action in the field, the Euclidean path integral $\Psi_+[\psi_1, \psi_2]$ with boundary conditions ψ_1 and ψ_2 specified on the foliations $\mathcal{S}_1 = \tau_1$ and $\mathcal{S}_2 = \tau_2$ respectively, can be accurately computed as follows

$$\Psi_+[\psi_1, \psi_2] = \left(\frac{\lambda}{2\pi \sinh\left(\frac{\lambda\beta}{2}\right)} \right)^{1/2} \exp \left[-\frac{\lambda}{2} \left((\psi_1^2 + \psi_2^2) \coth\left(\frac{\lambda\beta}{2}\right) - \frac{2\psi_1\psi_2}{\sinh\left(\frac{\lambda\beta}{2}\right)} \right) \right]. \quad (19)$$

The above result can be reformulated in terms of the n -excited state of the Harmonic Oscillator, utilizing Hermite polynomials $H_n(x)$,

$$\Psi_+[\psi_1, \psi_2] = \frac{1}{\sqrt{Z(\beta)}} \sum_{n=0}^{\infty} e^{-\frac{\beta}{2}E_n} \varphi_n(\psi_1) \varphi_n(\psi_2), \quad (20)$$

$$\varphi_n(\psi) = \left(\sqrt{\frac{\lambda}{\pi}} \frac{1}{2^n n!} \right)^{1/2} H_n(\sqrt{\lambda}\psi) e^{-\frac{\lambda}{2}\psi^2}, \quad (21)$$

where $E_n = \hbar\lambda(n + 1/2)$. In addition, the normalization factor Z depends on β ,

$$1 = \int_{-\infty}^{\infty} d\psi_1 d\psi_2 K_+[\psi_1, \psi_2] K_-[\psi_1, \psi_2] = \frac{1}{Z} \sum_{n=0}^{\infty} e^{-\beta E_n} \rightarrow Z = \sum_{n=0}^{\infty} e^{-\beta E_n}. \quad (22)$$

At this point, we note that the Euclidean path integral (20) corresponds to the ground state introduced by Umezawa and Takahashi, denoted as $|0(\beta)\rangle$, and better known as the thermofield double state (TFD) [11–14]. The meaning of this expression will be further explained in section 3.1.

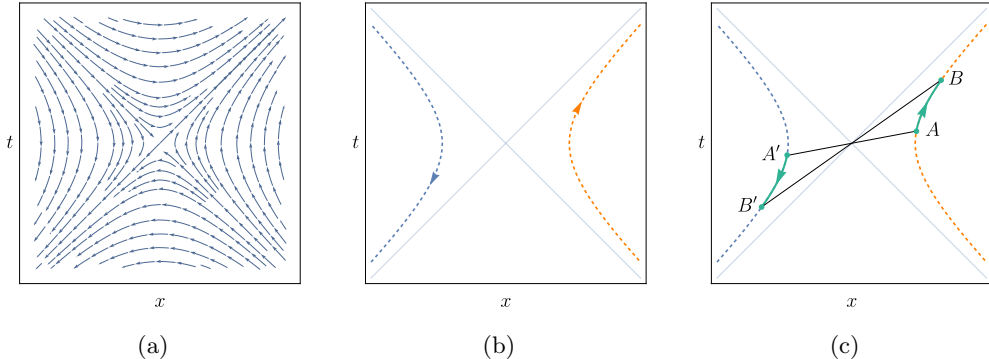


Figure 4: (a) Integral curves of the vector field ∂_τ on Minkowski spacetime. (b) Trajectories for a fixed value of ξ . (c) Evolution from A to B related by parity and time-reversal to that from A' to B' .

3.1. Thermofield Double State

To identify the fields ψ_1 and ψ_2 in (20) within the context of the causal diamond, we first revisit the analysis conducted in Rindler spacetime given by the transformation (8). From this, we have that the metric is independent of τ ,

$$ds^2 = -\frac{\xi^2}{\alpha^2} d\tau^2 + d\xi^2. \quad (23)$$

Hence, there is a Killing vector associated with the symmetry in temporal translations, denoted as ∂_τ , which in Minkowski coordinates is given by

$$\partial_\tau = \frac{\partial x}{\partial \tau} \partial_x + \frac{\partial t}{\partial \tau} \partial_t = \frac{1}{\alpha} (t \partial_x + x \partial_t). \quad (24)$$

We note that the generator of time evolution in Rindler spacetime corresponds to the boost generator in the x direction of Minkowski spacetime. The integral curves of this vector field are shown in figure 4a, where we observe forward time evolution in the right wedge and backward time evolution in the left wedge.

Similarly, it is important to mention that the trajectories described by the observer under constant acceleration, across the entire range of τ values, are given by the semi-hyperbolas in the right and left wedges, such that together they complement the hyperbola defined over the entire Minkowski spacetime (see figure 4b), whose asymptotes are given by the null horizons $t = \pm x$. Furthermore, the temporal evolution on one of the semi-hyperbolas automatically describes the other through parity and time-reversal transformations in $\{x, t\}$, as we note in figure 4c.

In Euclidean signature ($\tau \rightarrow -i\tau$), the vector field (24) becomes the generator of counterclockwise rotations in the Euclidean plane (see figure 5a),

$$\partial_\tau = \frac{1}{\alpha} (-t_E \partial_x + x \partial_{t_E}). \quad (25)$$

As a consequence of the Wick rotation, we have different trajectories compared to those seen in the Lorentzian case. Additionally, a periodicity in τ has been induced,

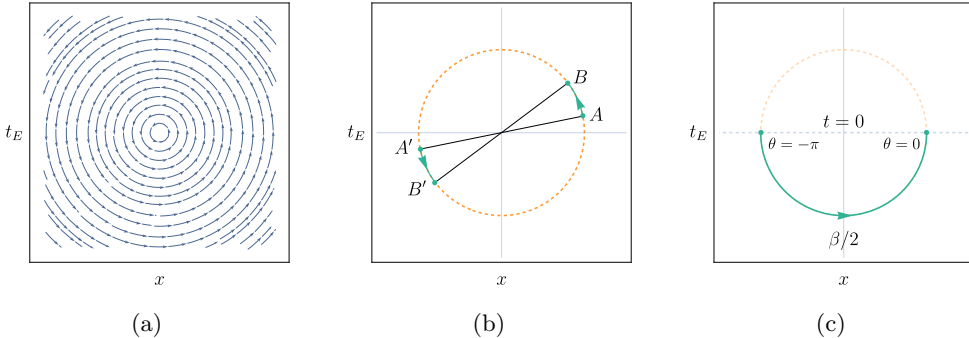


Figure 5: (a) Integral curves of the vector field $\partial\tau$ in the Euclidean plane. (b) Evolution from A to B related by parity and time-reversal to that from A' to B' . (c) Evolution by π radians in the lower half of the Euclidean plane.

since in the Euclidean plane, the transformations (8) are given in terms of $\sin(\tau/\alpha)$ and $\cos(\tau/\alpha)$. Furthermore, the trajectories obtained across the entire range of τ values do not ‘‘complement’’ each other in the sense we saw in the Lorentzian case, where both semi-hyperbolas formed a whole in the Minkowski plane. Here, for both the transformation cases in the left and right wedges, we obtain a circumference in the entire Euclidean plane, which means that this mapping is 2 to 1. However, complementarity is observed when analyzing τ evolution, as one trajectory immediately defines the other, again through parity and time-reversal transformations in $\{x, t_E\}$ (which in this case would also be parity in t_E), as shown in figure 5b.

This result is crucial as it provides a better understanding of the Euclidean path integral and the role of the cylinder in Laflamme’s proposal. As mentioned previously, we identify the manifold over which the action is defined as M_+ . Therefore, the evolution from τ_1 to τ_2 , precisely half the periodicity β , is interpreted as the propagation of Rindler fields observed in the Euclidean plane, involving a rotation of π radians. In other words, the evolution occurs from states defined in the left wedge (at $\theta = -\pi$) to those in the right wedge (at $\theta = 0$), where we consider the propagation precisely at $t = 0$, since the evolution in τ in the lower half of the Euclidean plane prepares the state for its evolution in Lorentzian time, where such connection occurs precisely at $t = t_E = 0$ (see figure 5c). Consequently, the Euclidean path integral (20) can be expressed as [33]

$$\Psi_+[\psi_L, \psi_R] = \langle \psi_R | e^{-\pi J} \Theta | \psi_L \rangle, \quad (26)$$

where we identify $\psi_1 = \psi_L$ and $\psi_2 = \psi_R$. Additionally, Θ is the anti-unitary *CPT* operator,

$$\Theta \psi_L \Theta^{-1} = \psi_R, \quad (27)$$

applied to the Rindler state in the left wedge, defined for $x < 0$ and evolving in t in reverse.

For the causal diamond, we use the mapping defined between the internal (external) region of the causal diamond and the right (left) Rindler wedge, given in (11). This allows us to implement this transformation at the quantum level using

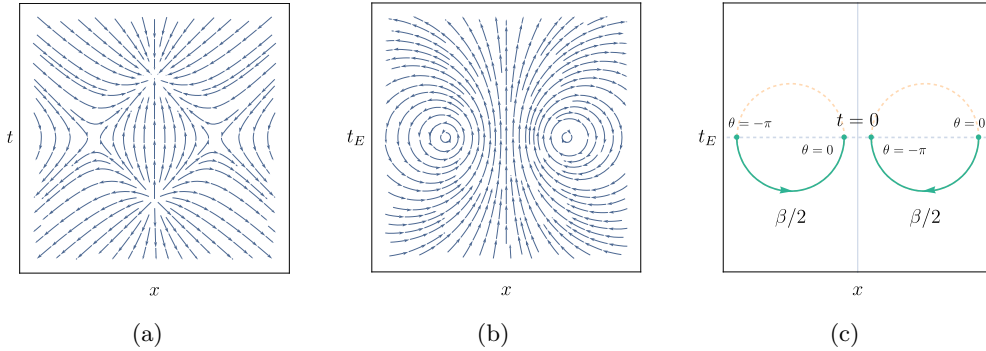


Figure 6: Integral curves of the vector field ∂_τ in (a) Minkowski and (b) Euclidean Plane. (c) Evolution by π radians in the lower half of the Euclidean plane.

the unitary operator

$$U = e^{-i(a^\alpha T_\alpha + b^\alpha K_\alpha)}, \quad (28)$$

where $b^\mu = (0, -\frac{1}{2\alpha})$ and $a^\mu = (0, -\alpha)$. Thus,

$$U\psi_R U^{-1} = \psi_{in}, \quad U\psi_L U^{-1} = \psi_{ext}. \quad (29)$$

Furthermore, from the action of the anti-unitary CPT operator Θ on the scalar fields in the left and right Rindler wedges, we obtain

$$\Theta_D = U\Theta U^{-1}, \quad (30)$$

from which we finally derive the anti-unitary operator Θ_D , which elaborates the map between the fields in the interior and exterior regions of the causal diamond,

$$\Theta_D \psi_{ext} \Theta_D^{-1} = \psi_{in}. \quad (31)$$

Applying (29) and (30) to (26), we find

$$\langle \psi_{in} | e^{-\pi J_D} \Theta_D | \psi_{ext} \rangle, \quad (32)$$

where $e^{-\pi J} \rightarrow e^{-\pi J_D} = U e^{-\pi J} U^{-1}$ is the conformal map that implements the rotation from the exterior region to the interior region of the causal diamond. This can be visualised by constructing the vector field $\partial_\tau = (\partial x^\mu / \partial \tau) \partial_\mu$ [34], taking into account the conformal transformation (6) (see figures 6a and 6b). In Euclidean signature, we have

$$\partial_\tau = \frac{1}{\alpha^2} \left(t_E x \partial_x + \frac{1}{2} (\alpha^2 + t_E^2 - x^2) \partial_{t_E} \right). \quad (33)$$

Therefore, we observe that (33) maps the exterior region to the interior of the causal diamond through rotations of π radians on each side of the Euclidean plane, which corresponds, each one, to $\beta/2$ for τ (see figure 6c).

In conclusion, the identifications $\psi_1 = \psi_{ext}$ and $\psi_2 = \psi_{int}$ naturally emerge. Thus, the Euclidean path integral (20) represents the thermofield double state, describing the thermal nature of the “vacuum” with a temperature given by $T = \beta^{-1}$. In bra-ket notation notation, we have

$$|TFD\rangle = \frac{1}{\sqrt{Z(\beta)}} \sum_{n=0}^{\infty} e^{-\frac{\beta}{2} E_n} |n_{in}\rangle \otimes \Theta_D |n_{ext}\rangle. \quad (34)$$

4. Density matrix and Diamond Temperature

The Thermofield Double State (20) manifests itself as an entangled state of the ψ_1 and ψ_2 states. Here, ψ_2 is the fictitious field introduced by Umezawa and Takahashi, which in this analysis arises naturally when implementing the considerations made regarding Euclidean geometry. Consequently, the physical system under analysis will be described by the reduced density matrix obtained by taking the partial trace of the total density matrix given by $\rho[\psi_1, \psi_2] = \Psi_+[\psi_1, \psi_2]\Psi_-[\psi_1, \psi_2]$. This is achieved by integrating out the fictitious field,

$$\rho[\psi_1] = \int_{-\infty}^{\infty} d\psi_2 \rho[\psi_1, \psi_2] = \frac{1}{Z(\beta)} \sum_{n=0}^{\infty} e^{-\beta E_n} \varphi_n(\psi_1) \varphi_n^*(\psi_1) = \frac{e^{-\beta H}}{Z(\beta)}. \quad (35)$$

As we can observe, the perception of the observer's ground state in a causal diamond is determined by a canonical ensemble in thermal equilibrium with a heat bath at temperature β^{-1} .

Additionally, from the analysis of the cylinder's geometry (section 2), we know that β represents the period of the coordinate τ . Thus, it becomes essential to employ a coordinate transformation between the latter and the plane to establish the temperature associated with this periodicity within the framework of causal diamond geometry. Furthermore, in the context of this ongoing study, we will confine our analysis to the scenario where the observer is located at $x = 0$. In this manner, the transformations are delineated as follows

$$\tau(t_E, 0) = \alpha \tan^{-1} \left(\frac{2\alpha t_E}{\alpha^2 - t_E^2} \right), \quad \xi(t_E, 0) = 2\alpha. \quad (36)$$

This allows us to express the conformal factor in terms of t_E and α , which is given by $\Omega(t_E) = \frac{1}{2} \left(\frac{\alpha^2 + t_E^2}{2\alpha^2} \right)$. Consequently, by identifying the line elements of the Diamond and the plane, $\Omega(t_E)^2 \frac{(2\alpha)^2}{\alpha^2} d\tau^2 = dt_E^2$, it becomes possible to determine the value of β as perceived by the observer situated at $x = 0$, whose lifetime is limited to $t_E \in (-\alpha, \alpha)$. Thus,

$$\int_0^{\beta} d\tau = \int_{-\alpha}^{+\alpha} \frac{dt_E}{\left(\frac{\alpha^2 + t_E^2}{2\alpha^2} \right)} \quad \beta = \pi\alpha. \quad (37)$$

The temperature detected by the diamond observer is then given by $T = 1/(\pi\alpha)$, which is exactly the diamond temperature found in the literature.

5. Conclusions

This article adds to a series of studies on the temperature of causal diamonds. The temperature perceived by a diamond observer has been obtained using the modular flow and thermal time hypothesis approach [18], Bogolyubov transformations [30], Unruh-deWitt detector formalism [28, 30], open quantum systems approach [31], among many others, and now, in this paper, using a path integral formalism. All these

derivations lead to the same diamond temperature, which confirms the robustness of this result. It also corroborates the fact that the causal diamond thermality has all the characteristics of the Unruh effect even in the absence of acceleration, thus highlighting the fact that the study of causal diamonds demands more attention from the community. Recently, it has been established that conformal Killing vectors in the causal diamond geometry are closely related to the generators of $sl(2, \mathbb{R})$ algebra in (0+1)-D conformal field theory, known as conformal quantum mechanics [23, 34–40]. On the other hand, conformal quantum mechanics plays an integral role in determining the temperature of black hole radiation [41–46], thus tying causal diamonds to the near-horizon physics of black holes more closely. Causal diamonds are also intriguing due to their connection with entanglement entropy in many-body systems and quantum chaos. These connections imply that causal diamonds can be the key to understanding the origin of black hole entropy and information scrambling in black holes. We intend to explore some of these topics in the future.

Acknowledgments

Two of the authors, C.R.O. and G.V-M. would like to thank Pablo Lopez-Duque for illuminating discussions on the geometry of causal diamonds. C.R.O. and G.V-M. were partially supported by the Army Research Office (ARO), Grant W911NF-23-1-0202.

Appendix A. Computation of the Euclidean Action

Using the Fourier transformation for the real scalar field ϕ ,

$$\phi(\tau, \rho) = \frac{1}{2\pi} \int e^{i\rho\lambda} \phi(\tau, \lambda) d\lambda, \quad (\text{A.1})$$

in the action (13), we have

$$\begin{aligned} S_E[\phi] &= -\frac{1}{2} \int d\rho d\tau \frac{1}{\sqrt{2\pi}} \int e^{i\rho\lambda_1} \phi(\tau, \lambda_1) d\lambda_1 [\partial_\tau^2 + \partial_\rho^2] \frac{1}{\sqrt{2\pi}} \int e^{-i\rho\lambda_2} \phi^*(\tau, \lambda_2) d\lambda_2 \\ &= -\frac{1}{2} \int d\tau d\lambda_1 d\lambda_2 \left[\frac{1}{2\pi} \int d\rho e^{i\rho(\lambda_1 - \lambda_2)} \right] \phi(\tau, \lambda_1) [\partial_\tau^2 - \lambda_2^2] \phi^*(\tau, \lambda_2) \\ &= -\frac{1}{2} \int d\tau d\lambda_1 d\lambda_2 \delta(\lambda_1 - \lambda_2) \phi(\tau, \lambda_1) [\partial_\tau^2 - \lambda_2^2] \phi^*(\tau, \lambda_2) \\ &= -\frac{1}{2} \int d\tau d\lambda \phi(\tau, \lambda) [\partial_\tau^2 - \lambda^2] \phi^*(\tau, \lambda). \end{aligned} \quad (\text{A.2})$$

The path integral for this action, in discrete form, is proportional to

$$\prod_{i,\alpha} \int d\phi_{i\alpha} e^{\frac{1}{2} \Delta\lambda_\alpha \Delta\tau_i \phi_{i\beta} D_{\beta j} \phi_{j\alpha}^*}$$

As mentioned in section 2.2, a fundamental requirement for the applicability of the Laflamme method is periodicity in τ , given by $\tau \sim \tau + \beta$. Therefore, in the product over τ_i , we will make a distinction for the manifolds M_+ and M_- , denoted by $0 < i < \beta/2$ and $\beta/2 < i < \beta$, respectively. We have

$$P_{\text{dis}} \propto \prod_{\alpha} \prod_{0 < i < \beta/2} \int d\phi_{i\alpha} e^{\frac{1}{2} \Delta\lambda_\alpha \Delta\tau_i \phi_{i\beta} D_{\beta j} \phi_{j\alpha}^*} \prod_{\alpha} \prod_{\beta/2 < i' < \beta} \int d\phi_{i'\alpha} e^{\frac{1}{2} \Delta\lambda_\alpha \Delta\tau'_i \phi_{i'\beta} D_{\beta j} \phi_{j\alpha}^*}.$$

Taking the limit $\Delta\tau_i \rightarrow 0$, we obtain

$$P_{\text{dis}} \propto \prod_{\alpha} \int_{\mathcal{C}_+} d\phi_{\alpha} e^{\frac{1}{2}\Delta\lambda_{\alpha} \int d\tau \phi_{\alpha}(\tau)(\partial_{\tau}^2 - \lambda_{\alpha}^2)\phi_{\alpha}^*(\tau)} \prod_{\alpha} \int_{\mathcal{C}_-} d\phi_{\alpha} e^{\frac{1}{2}\Delta\lambda_{\alpha} \int d\tau \phi_{\alpha}(\tau)(\partial_{\tau}^2 - \lambda_{\alpha}^2)\phi_{\alpha}^*(\tau)}.$$

We note that the factor $\Delta\lambda_{\alpha}\phi_{\alpha}(\tau)\partial_{\tau}^2\phi_{\alpha}^*(\tau)$, through integration by parts and considering that $\phi_{\alpha}(\tau) \rightarrow 0$ as $\tau \rightarrow \pm\infty$, leaves us with the term $-\Delta\lambda_{\alpha}|\partial_{\tau}\phi(\tau)|^2$ in the integral, which is real and can be rewritten as $-[\partial_{\tau}\psi_{\alpha}(\tau)]^2$, which again, through integration by parts, leaves us with $\psi_{\alpha}(\tau)\partial_{\tau}^2\psi_{\alpha}(\tau)$. Similarly, the term $-\lambda_{\alpha}^2\Delta\lambda_{\alpha}|\phi(\tau)|^2$ can be rewritten as $-\lambda_{\alpha}^2\psi_{\alpha}^2(\tau)$. Consequently, for the weight of the integral, we have $D_{\phi_{\alpha}} \rightarrow D_{\psi_{\alpha}} = |J|D_{\phi_{\alpha}}$, where J is the Jacobian for the transformation $\phi_{\alpha} \rightarrow \psi_{\alpha}$. Therefore, we have

$$P_{\text{dis}} = \prod_{\lambda} \int_{\mathcal{C}_+} D\psi_{\lambda} e^{-S_E[\psi_{\lambda}]} \prod_{\lambda} \int_{\mathcal{C}_-} d\phi_{\lambda} e^{-S_E[\psi_{\lambda}]}, \quad (\text{A.3})$$

where $S_E[\psi_{\lambda}]$ is the harmonic oscillator action for each single mode λ ,

$$S_E[\psi_{\lambda}] = -\frac{1}{2} \int d\tau \psi_{\lambda}(\tau) [\partial_{\tau}^2 - \lambda^2] \psi_{\lambda}(\tau). \quad (\text{A.4})$$

References

- [1] Hawking S W 1974 *Nature* **248** 30–31
- [2] Hawking S W 1975 *Communications in mathematical physics* **43** 199–220
- [3] Hawking S W 1976 *Phys. Rev. D* **13** 191–197
- [4] Unruh W G 1976 *Phys. Rev. D* **14** 870
- [5] Davies P C W, Fulling S A and Unruh W G 1976 *Phys. Rev. D* **13** 2720–2723
- [6] Davies P C W and Fulling S A 1976 *Proc. Roy. Soc. Lond. A* **348** 393–414
- [7] Davies P C W 1977 *Proc. Roy. Soc. Lond. A* **353** 499–521
- [8] Davies P C W 1975 *J. Phys. A* **8** 609–616
- [9] Wald R M 1975 *Commun. Math. Phys.* **45** 9–34
- [10] Parker L 1975 *Phys. Rev. D* **12** 1519–1525
- [11] Takahashi Y and Umezawa H 1975 *Collect. Phenom.* **2** 55–80
- [12] Takahashi Y and Umezawa H 1996 *Int. J. Mod. Phys. B* **10** 1755–1805
- [13] Umezawa H, Matsumoto H and Tachiki M 1982 *THERMO FIELD DYNAMICS AND CONDENSED STATES*
- [14] Matsumoto H, Nakano Y, Umezawa H, Mancini F and Marinaro M 1983 *Prog. Theor. Phys.* **70** 599–602
- [15] Israel W 1976 *Phys. Lett. A* **57** 107–110
- [16] Laflamme R 1989 *Physica A* **158** 58–63
- [17] Laflamme R 1989 *Nucl. Phys. B* **324** 233–252
- [18] Martinetti P and Rovelli C 2003 *Class. Quant. Grav.* **20** 4919–4932
- [19] Martinetti P 2009 *Mod. Phys. Lett. A* **24** 1473–1483
- [20] Jacobson T and Visser M 2019 *SciPost Phys.* **7** 079
- [21] Jacobson T and Visser M R 2023 *SciPost Phys.* **15** 023
- [22] Wang J 2019 *Phys. Rev. D* **100** 064020
- [23] Arzano M 2020 *JHEP* **05** 072
- [24] Banks T 2023 *International Journal of Modern Physics D* **32** 2341002
- [25] Chandrasekaran V and Prabhu K 2019 *JHEP* **10** 229
- [26] de Boer J, Haehl F M, Heller M P and Myers R C 2016 *JHEP* **08** 162
- [27] Gibbons G W and Solodukhin S N 2007 *Phys. Lett. B* **649** 317–324
- [28] Foo J, Onoe S, Zych M and Ralph T C 2020 *New J. Phys.* **22** 083075
- [29] Andrade e Silva R and Jacobson T 2023 *Phys. Rev. D* **107** 024033
- [30] Su D and Ralph T C 2016 *Phys. Rev. D* **93** 044023
- [31] Chakraborty A, Camblong H and Ordóñez C 2022 *Phys. Rev. D* **106** 045027
- [32] Camblong H, Chakraborty A, Lopez-Duque P and Ordóñez C 2024 *Phys. Rev. D* **109** 105003

- [33] Harlow D 2016 *Rev. Mod. Phys.* **88** 015002
- [34] Jacobson T 2016 *Phys. Rev. Lett.* **116** 201101
- [35] Arzano M 2021 *Journal of High Energy Physics* **2021** 1–14
- [36] Arzano M, D’Alise A and Frattulillo D 2023 *Journal of High Energy Physics* **2023** 1–17
- [37] De Lorenzo T and Perez A 2018 *Phys. Rev. D* **97** 044052
- [38] De Lorenzo T and Perez A 2019 *Phys. Rev. D* **99** 065009
- [39] Herrero A and Morales J A 1999 *Journal of Mathematical Physics* **40** 3499–3508
- [40] Arzano M, D’Alise A and Frattulillo D 2024 *arXiv:2405.02623*
- [41] Camblong H E and Ordóñez C R 2005 *Phys. Rev. D* **71** 104029
- [42] Camblong H E and Ordóñez C R 2005 *Phys. Rev. D* **71** 124040
- [43] Camblong H E, Chakraborty A and Ordóñez C R 2020 *Phys. Rev. D* **102** 085010
- [44] Azizi A, Camblong H, Chakraborty A, Ordóñez C and Scully M 2021 *Phys. Rev. D* **104** 065006
- [45] Azizi A, Camblong H, Chakraborty A, Ordóñez C and Scully M 2021 *Phys. Rev. D* **104** 084086
- [46] Azizi A, Camblong H, Chakraborty A, Ordóñez C and Scully M 2021 *Phys. Rev. D* **104** 084085